Ab initio study of electron capture in low-energy collisions of N^{4+} with hydrogen

B. Zygelman* and P. C. Stancil†
W. M. Keck Laboratory for Computational Physics, Department of Physics, University of Nevada at Las Vegas, Las Vegas, Nevada 89154

N. J. Clarke‡ and D. L. Cooper§
Department of Chemistry, University of Liverpool, P.O. Box 147, Liverpool L69 3BX, United Kingdom
(Received 22 October 1996; revised manuscript received 21 March 1997)

We present cross sections for the direct charge-transfer process $N^{4+}(2s)+H\rightarrow N^{3+}(nl;n'l')+H^{+}$ for center-of-mass collision energies between 0.1 eV/amu and 8 keV/amu. The results are in good agreement, at low energies, with merged-beams measurements for the total electron-capture cross sections in collisions of N^{4+} with hydrogen and deuterium targets. We also compare the calculated final-state cross sections with the results of recent translational energy spectroscopy measurements. The calculated final-state cross sections show good agreement with the experiment for ion projectile energies up to 8 keV. Our calculations suggest that the total electron-capture cross sections display Langevin behavior for collision energies below 0.4 eV/amu. [S1050-2947(97)05807-1]

PACS number(s): 34.70. +e

I. INTRODUCTION

The electron-capture process

$$N^{4+}(2s)+H\rightarrow N^{3+}(nl;n'l')+H^{+} \tag{1}$$

has received considerable attention in recent years [1–8]. Process (1) plays an important role in determining the ionization stages of nitrogen in various astrophysical environments [1,2], and is a major mechanism for populating the excited states of the N^{3+} ion whose line emissions have been observed in planetary nebulae, symbiotic stars, and supernova remnants [9,10].

Estimates for the total electron-capture rate coefficients have been given for temperatures in the range $1000\ \mathrm{K}<T<30\,000\ \mathrm{K}$ [1], and Feickert *et al.* [2] calculated cross sections and rate coefficients that spanned temperatures from 30 K to $\approx 10^5$ K. In that calculation, the molecular potential surfaces and nonadiabatic couplings, for the NH^{4+} quasimolecule that is formed during the collision, were constructed with a method that is based on general and nonrigorous assumptions. Uncertainty in the molecular data used in those calculations, translates into a corresponding uncertainty in the reported cross sections and rate coefficients.

Total charge-capture cross sections for the process

$$N^{4+}+H\rightarrow N^{3+}+H^{+} \tag{2}$$

have been measured, using merged-beam techniques, by Huq, Havener, and Phaneuf [3], and Folkerts *et al.* [6]. The total capture cross section is a sum of the partial cross sections for capture into the $nl;n'l'$ states of the N^{3+} ion. For the process given by Eq. (1), and at low energies, it is valid to restrict the sum to contributions from the $nl=2s,2p$; $n'l'=3s,3p$ and $3d$ states of the N^{3+} ion only [5]. Capture into both the singlet and triplet manifolds of the N^{3+} ion must be accounted for, since the merged-beam experiments cannot distinguish capture into states of specific spin. Comparison of the measured data [3] show fair agreement with the calculated cross sections of Feickert *et al.* [11].

Shimakura, Itoh, and Kimura [4] calculated the state-to-state cross sections for process (1) using a semiclassical method for collision energies from 10 eV≈10 keV, while for energies below 10 eV/amu they used a two-channel quantum-mechanical method, with molecular potentials and couplings obtained by a model potential approach. An *ab initio* theory for electron capture into the singlet states of $N^{3+}(2s3l'),l'=s,p,d$, following the initial approach of the N^{4+} ion and hydrogen, was presented by Zygelman *et al.* [5]. In that calculation, all molecular surfaces and nonadiabatic couplings for the molecular states that asymptotically correlate to the $H^{+}+N^{3+}(2s3l'=s,p,d)$ atomic fragments were generated with *ab initio* methods. Though the results of the calculation for the total cross sections given by Shimakura, Itoh, and Kimura are in good agreement with the experimental values reported by Huq, Havener, and Phaneuf, the calculation of Zygelman *et al.* give singlet cross sections that increase as the collision energy decreases, in contrast to the experimental evidence that the total cross sections monotonically decrease at low energies. A recent, more detailed, theoretical study [6] confirmed the theoretical predictions of their earlier calculation [4], that the total capture cross sections of the NH^{4+} collision system monotonically decrease at low collision energies.

There have been several experimental attempts in the past few years to observe the predictions of the Langevin model; i.e., capture cross sections that have a $1/v$ dependence at low energies and, as a consequence, rate coefficients that tend to a constant as temperatures decrease. A few systems that exhibit Langevin behavior have been identified [13] but the

*Electronic address: bernard@physics.unlv.edu
†Electronic address: stancil@mail.phy.ornl.edu
‡Electronic address: nickc@tcpc.bham.ac.uk
§Electronic address: dlc@rs2.ch.liv.ac.uk

TABLE I. SCVB adiabatic potential-energy curves for the seven lowest $^3\Sigma^+$ states of NH^{4+}. Energies are given in atomic units.

$R(a_0)$	$(1)^3\Sigma^+$	$(2)^3\Sigma^+$	$(3)^3\Sigma^+$	$(4)^3\Sigma^+$	$(5)^3\Sigma^+$	$(6)^3\Sigma^+$	$(7)^3\Sigma^+$
2.00	−49.473 022	−48.315 939	−47.951 746	−47.823 050	−47.702 854	−47.397 736	−47.384 510
2.50	−49.721 366	−48.648 186	−48.287 214	−48.135 700	−48.008 546	−47.743 483	−47.742 868
3.00	−49.897 045	−48.807 200	−48.436 592	−48.352 433	−48.220 760	−48.017 126	−47.960 484
3.25	−49.967 671	−48.851 473	−48.477 648	−48.437 565	−48.304 001	−48.147 683	−48.039 878
3.50	−50.029 293	−48.881 768	−48.513 984	−48.504 511	−48.376 358	−48.261 243	−48.106 370
3.75	−50.083 168	−48.902 016	−48.576 290	−48.525 855	−48.436 294	−48.351 695	−48.163 148
4.00	−50.130 898	−48.915 985	−48.632 925	−48.539 340	−48.494 245	−48.429 597	−48.213 114
4.25	−50.173 310	−48.925 248	−48.682 502	−48.549 040	−48.545 117	−48.494 118	−48.261 243
4.50	−50.211 229	−48.931 720	−48.725 862	−48.592 527	−48.562 333	−48.540 268	−48.304 296
4.75	−50.245 326	−48.936 830	−48.763 375	−48.635 734	−48.598 625	−48.553 045	−48.342 331
5.00	−50.276 160	−48.941 980	−48.795 055	−48.674 394	−48.635 580	−48.557 300	−48.375 381
5.25	−50.304 135	−48.947 993	−48.821 144	−48.708 090	−48.668 444	−48.559 659	−48.403 482
5.50	−50.329 603	−48.955 968	−48.841 866	−48.737 765	−48.697 437	−48.563 926	−48.427 502
5.75	−50.352 906	−48.966 261	−48.857 594	−48.763 179	−48.723 287	−48.570 422	−48.448 264
6.00	−50.374 299	−48.978 564	−48.869 690	−48.784 274	−48.746 504	−48.579 156	−48.466 732
6.25	−50.393 998	−48.992 147	−48.879 983	−48.801 054	−48.767 390	−48.589 819	−48.483 906
6.50	−50.412 194	−49.006 215	−48.890 050	−48.813 791	−48.786 046	−48.601 749	−48.501 145
6.75	−50.429 050	−49.020 139	−48.900 688	−48.823 506	−48.802 135	−48.614 192	−48.518 033
7.00	−50.444 705	−49.033 544	−48.911 883	−48.832 499	−48.814 407	−48.626 479	−48.533 728
7.25	−50.459 197	−49.045 734	−48.923 130	−48.843 254	−48.821 225	−48.636 927	−48.548 358
7.50	−50.472 853	−49.058 307	−48.934 587	−48.855 506	−48.824 579	−48.649 142	−48.562 026
7.75	−50.485 649	−49.070 274	−48.945 803	−48.867 787	−48.826 116	−48.661 073	−48.574 824
8.00	−50.497 671	−49.081 643	−48.956 654	−48.879 624	−48.826 769	−48.672 745	−48.586 832
9.00	−50.538 889	−49.121 424	−48.995 017	−48.921 026	−48.826 349	−48.708 644	−48.628 239
10.00	−50.572 254	−49.154 084	−49.027 111	−48.954 590	−48.825 370	−48.742 932	−48.661 403
12.00	−50.622 200	−49.203 655	−49.075 752	−49.004 886	−48.824 385	−48.793 072	−48.711 183
13.00	−50.641 254	−49.222 448	−49.094 413	−49.024 110	−48.823 861	−48.811 763	−48.730 336
13.72	−50.653 278	−49.234 381	−49.106 223	−49.036 199	−48.823 600	−48.823 510	−48.742 399
14.00	−50.657 640	−49.238 715	−49.110 512	−49.040 568	−48.827 892	−48.823 482	−48.746 755
16.00	−50.684 370	−49.265 293	−49.136 857	−49.067 311	−48.854 282	−48.823 374	−48.773 437
20.00	−50.721 817	−49.302 613	−49.173 933	−49.104 745	−48.891 422	−48.823 336	−48.810 797

observations in Refs. [4,6] seem to preclude this possibility for the NH^{4+} system. Because of the behavior of the calculated singlet cross sections at low energies, we suggested [5] that the NH^{4+} system may serve as an additional candidate for the experimental observation of Langevin behavior. It was pointed out [5] that the apparent disagreement between theory [5] and experiment [3] may be the failure in the assumption that the cross sections at low energy are independent of the spin multiplicity of the molecular potentials in which the collision partners evolve. Until a separate calculation involving the triplet molecular potentials and couplings is performed, comparison with the experimental values for the total cross sections for process (2) is necessarily tentative.

The purpose of this paper is to report the results of such a calculation. In Sec. II we outline and summarize the results of the *ab initio* calculations for the adiabatic potential surfaces, along with the nonadiabatic radial couplings, for the NH^{4+} triplet system. In Sec. III we review the quantal collision theory used in this calculation and in Sec. IV we discuss and summarize our calculations for the state-to-state cross sections. We combine and extend the results of our previous calculation [5] to estimate the total charge-transfer cross sections for process (2). We find good agreement with experiments at low energies. However, our results suggest that the total capture cross sections will eventually increase, for energies <0.4 eV/amu, in contrast to the conclusions of Shimakura, Itoh, and Kimura [4] and Folkerts *et al.* [6].

We also compare our state-to-state cross sections with the results of a recent measurement by McCullough *et al.* [8] using translational energy spectroscopy. The measurements are taken for N^{+4} projectile energies ranging from 4 keV to 24 keV. Our calculated final-state cross sections are shown to be in good agreement with the measured values for lab energies up to 8 keV. Atomic units are used throughout, unless otherwise noted.

II. SCVB CALCULATIONS

The spin-coupled valence-bond (SCVB) approach was used to calculate the relevant $^3\Sigma^+$ potential-energy curves and radial couplings necessary to perform the collision calculations for process (1). The approach very closely follows that employed previously for the $^1\Sigma^+$ states of NH^{4+} [5]. Not only did we use the same basis set as in Ref. [5], but we chose to expand the SCVB wave functions in configurations generated using the same classes of excitations and built from exactly the same set of $^1\Sigma^+$ orbitals. This strategy

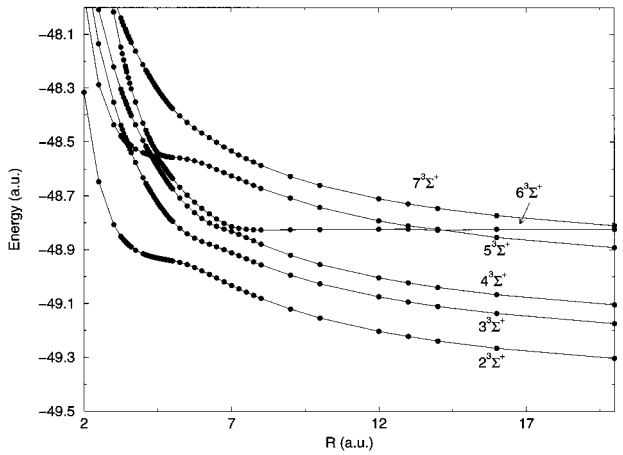

FIG. 1. Calculated adiabatic potential-energy curves (filled circles) for the triplet states of the NH^{4+} molecular ion.

leads to a total of 155 spatial configurations (279 VB structures) of $^3\Sigma^+$ symmetry. The resulting adiabatic potential-energy curves are presented in Table I and Fig. 1 for 31 nuclear separations R from $2a_0$ to $20a_0$. Each curve is labeled by a numeral, ranging from (1)–(7), in order of increasing energy. In Table II we tabulate the asymptotic energies of the first seven states, which span an energy range greater than 55 eV. Bearing in mind the very modest number of configurations used in the SCVB expansion, the level of agreement with the experimental values is impressive, with most of the asymptotes matching within 0.1 eV. The largest difference (0.232 eV) is for the $N^{3+}(2p3s;^3P)+H^+$ channel, which does not play a significant role in process (1). We present in Table III selected d/dR coupling matrix elements,

$$\mathcal{A}(i,j)\equiv\langle\phi_i|d/dR|\phi_j\rangle, \tag{3}$$

where ϕ_i is the adiabatic electronic wave function for state i, and the angle bracket notation implies integration over electronic coordinates. The resulting matrix elements are functions of nuclear separation R. The value $\mathcal{A}(i,j)$ depends on the choice of origin for the electronic coordinates, however, it was shown in Ref. [5] that the resulting scattering equations are actually independent of the choice of electronic coordinates within our Jacobi coordinate system. In our calculations we chose the origin for the electronic coordinates to be situated on the nuclear center of mass. Below we summarize the scattering equations, described in detail in Ref. [5], used in the present study.

The collision equations are solved in the diabatic picture [5] which may be obtained by a unitary phase, or gauge, transformation of the adiabatic potential curves (see discussion below). The diabatic potentials, for the triplet manifold of the NH^{4+} system are illustrated in Fig. 2(a), we also present, in Fig. 2(b), the diabatic potentials for the singlet manifold which are constructed from the adiabatic potentials and couplings given in Ref. [5].

III. SCATTERING FORMALISM

The cross sections are calculated using a quantum-mechanical close-coupling theory that has been described in detail in Ref. [5] and, for the sake of completeness, we briefly review it below.

TABLE II. Asymptotic energies (in eV) of the seven lowest $^3\Sigma^+$ states of NH^{4+}. The experimental energies are taken from Moore's table [14].

Asymptote	SCVB calculation	experiment	difference
$N^{3+}(2s2p;\ ^3P^o)+H^+$	−55.742	−55.529	−0.213
$N^{3+}(2s3s;\ ^3S)+H^+$	−17.126	−17.092	−0.034
$N^{3+}(2s3p;\ ^3P^o)+H^+$	−13.624	−13.533	−0.091
$N^{3+}(2s3d;\ ^3D)+H^+$	−11.742	−11.781	0.039
$N^{3+}(2p3s;\ ^3P^o)+H^+$	−5.937	−6.169	0.232
$N^{3+}(2p3p;\ ^3D)+H^+$	−3.741	−3.785	0.044
$N^{4+}(2s;\ ^2S)+H(1s)$	0.0	0.0	

The total wave function for the ion-atom system (after the center-of-mass motion has been factored out), may be expressed by the close-coupling expansion,

$$\Psi(\mathbf{R},\mathbf{r})=\sum_\gamma F_\gamma(\mathbf{R})\,\phi_\gamma(\mathbf{R},\mathbf{r}), \tag{4}$$

where $\phi_\gamma(\mathbf{R},\mathbf{r})$ are the eigenfunctions of the adiabatic Hamiltonian [5], $F_\gamma(\mathbf{R})$ is an effective scattering amplitude for channel γ, and $\mathbf{R}$ is the internuclear separation vector for the ion-atom system. In practice, the infinite sum (4) must be truncated so that the resulting coupled equations remain tractable. We include, in this sum, all open channels of the NH^{4+} system that are connected by the radial coupling operator described below. In this approximation, we neglect effects induced by couplings into closed channels and angular couplings among the open channels. The latter become important at higher collision energies and have been included in the semiclassical collision study of Ref. [4]. At the collision energies of interest here these effects are not significant [4,6].

Following the procedure outlined in Ref. [5] we derive the coupled equations

$$-\frac{1}{2\mu}[\underline{I}\boldsymbol{\nabla}_R-i\underline{\mathbf{A}}(\mathbf{R})]^2\underline{F}(\mathbf{R})+\underline{V}(R)\underline{F}(\mathbf{R})=E\underline{F}(\mathbf{R}), \tag{5}$$

where $\underline{F}(\mathbf{R})$ is a column matrix whose elements are the channel amplitudes $F_\gamma(\mathbf{R})$, $\underline{V}(R)$ is a diagonal matrix whose elements consist of the Born-Oppenheimer potential-energy functions [15] for each channel state, and $\underline{\mathbf{A}}(R)$ is a Hermitian, antisymmetric, matrix whose elements are defined [5]

$$[\underline{\mathbf{A}}(R)]_{ab}\equiv i\langle\phi_a|\boldsymbol{\nabla}_R|\phi_b\rangle. \tag{6}$$

μ is the nuclear reduced mass and E is the collision energy in the center-of-mass frame. In this, the adiabatic description transitions are driven by the elements of the vector potential $\underline{\mathbf{A}}(R)$. In general, the vector potential contains both angular and radial components; since radial coupling is the primary mechanism in which transitions are induced at low collision energies, we neglect angular couplings. In that case, we can apply a unitary, or gauge, transformation on the amplitudes F_γ,

TABLE III. Selected matrix elements of d/dR between the first seven $^3\Sigma^+$ states of NH^{4+} in atomic units. The matrix indices correspond to the labels given in Table I.

$R(a_0)$	$\mathcal{A}(3,2)$	$\mathcal{A}(4,2)$	$\mathcal{A}(4,3)$	$\mathcal{A}(5,3)$	$\mathcal{A}(5,4)$	$\mathcal{A}(6,5)$
2.00	0.489 93	0.032 93	0.297 58	0.005 45	0.251 60	0.070 13
2.50	0.218 28	0.021 30	0.022 68	0.023 19	0.164 00	0.030 28
3.00	0.095 63	0.056 71	0.073 50	0.023 47	0.106 43	0.054 78
3.25	0.074 91	0.066 64	0.422 47	0.027 00	0.074 04	0.115 75
3.30	0.071 87	0.068 08	0.706 10	0.028 18	0.067 63	0.129 63
3.35	0.070 94	0.068 17	1.359 49	0.030 38	0.060 60	0.144 82
3.40	0.074 48	0.064 27	3.306 54	0.035 01	0.051 61	0.161 50
3.425	0.079 79	0.057 89	5.738 42	0.039 34	0.044 88	0.170 46
3.45	0.088 56	0.044 07	9.645 43	0.045 54	0.034 29	0.179 85
3.50	0.099 97	0.000 07	7.479 65	0.051 42	0.005 32	0.200 06
3.55	0.099 81	0.018 44	2.543 79	0.045 81	0.007 48	0.222 29
3.60	0.100 78	0.023 45	1.125 79	0.039 38	0.011 77	0.246 66
3.75	0.115 76	0.012 57	0.279 19	0.020 47	0.033 94	0.267 69
4.00	0.138 33	0.016 17	0.060 77	0.002 01	0.007 69	0.456 42
4.15	0.153 41	0.019 70	0.017 30	0.007 43	0.342 40	0.511 18
4.20	0.159 78	0.022 23	0.007 75	0.010 71	1.155 25	0.500 18
4.225	0.163 20	0.025 46	0.002 81	0.012 06	2.786 79	0.464 37
4.24	0.165 32	0.029 53	0.000 60	0.012 58	5.771 06	0.408 12
4.25	0.166 76	0.034 59	0.003 39	0.012 57	10.793 99	0.328 62
4.30	0.174 32	0.070 91	0.016 95	0.005 06	6.238 99	0.947 90
4.35	0.182 43	0.072 29	0.018 76	0.017 04	0.806 81	1.554 10
4.40	0.191 11	0.074 20	0.019 84	0.029 81	0.114 26	2.379 48
4.45	0.200 38	0.076 36	0.020 14	0.045 06	0.153 57	3.421 38
4.50	0.210 26	0.078 65	0.019 57	0.060 75	0.321 93	4.009 99
4.55	0.220 76	0.081 03	0.018 09	0.071 60	0.426 71	3.455 95
4.60	0.231 90	0.083 47	0.015 64	0.075 49	0.473 85	2.424 56
4.65	0.243 67	0.085 94	0.012 15	0.074 63	0.483 65	1.612 43
4.70	0.256 06	0.088 40	0.007 55	0.071 36	0.473 56	1.093 00
4.80	0.282 60	0.093 04	0.005 50	0.061 93	0.426 99	0.563 06
4.90	0.311 91	0.096 77	0.024 91	0.051 21	0.361 90	0.332 71
5.00	0.346 68	0.102 48	0.049 08	0.041 66	0.289 52	0.221 61
5.25	0.430 59	0.127 89	0.098 00	0.022 54	0.174 39	0.085 65
5.50	0.476 63	0.141 11	0.173 09	0.002 68	0.083 86	0.041 69
5.75	0.462 84	0.146 13	0.269 82	0.016 46	0.004 89	0.023 13
6.00	0.395 38	0.143 06	0.371 96	0.036 30	0.077 89	0.014 33
6.25	0.308 51	0.132 78	0.450 03	0.058 61	0.195 09	0.010 15
6.50	0.230 44	0.116 30	0.466 81	0.087 12	0.412 27	0.008 17
6.75	0.172 83	0.094 09	0.407 98	0.130 41	0.848 51	0.007 28
7.00	0.133 76	0.066 53	0.295 32	0.181 28	1.322 35	0.004 63
7.25	0.103 10	0.039 68	0.188 36	0.190 87	0.933 27	0.001 94
7.50	0.083 06	0.024 88	0.126 95	0.160 06	0.473 77	0.003 05
7.75	0.068 79	0.017 24	0.095 41	0.123 85	0.253 24	0.004 37
8.00	0.058 31	0.012 70	0.077 54	0.093 23	0.151 71	0.005 54
9.00	0.035 23	0.006 56	0.047 18	0.029 11	0.036 80	0.004 95
10.00	0.025 08	0.003 97	0.032 27	0.009 97	0.008 37	0.002 78
12.00	0.014 13	0.001 75	0.018 36	0.001 14	0.000 74	0.000 52
13.00	0.011 30	0.001 62	0.015 64	0.000 37	0.000 20	0.001 93
13.715	0.009 19	0.001 42	0.012 27	0.000 16	0.000 40	207.407 6
14.00	0.008 63	0.001 35	0.011 52	0.000 08	0.000 59	0.014 42

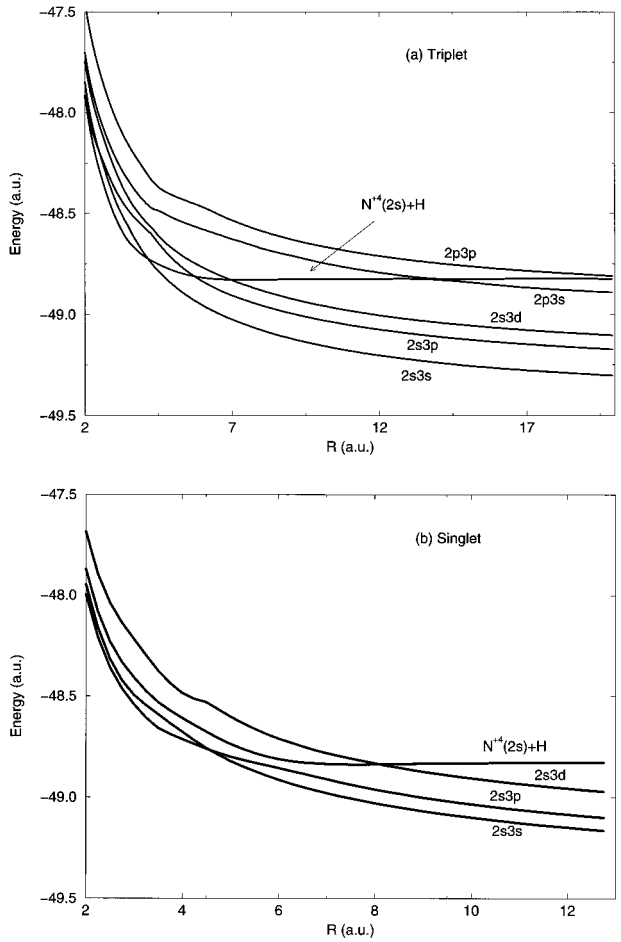

FIG. 2. Diabatic potential-energy curves of the NH^{4+} molecular ion. (a) $^3\Sigma^+$ states. (b) $^1\Sigma^+$ states (constructed from adiabatic potentials and couplings given in Ref. [5]).

$$\underline{F}(\mathbf{R}) = \underline{W}^{-1}\underline{G}(\mathbf{R}), \tag{7}$$

where $W(R)$ is a unitary matrix that is a solution to the first-order coupled equation [15]

$$0 = \underline{W}\,\underline{A}(R) - i\frac{d\underline{W}}{dR}. \tag{8}$$

Carrying out this transformation we arrive at the diabatic picture, in which, the amplitudes $\underline{G}(\mathbf{R})$ obey the coupled equation [16]

$$-\frac{1}{2\mu}\underline{I}\nabla_R^2\underline{G}(\mathbf{R}) + \underline{U}(R)\underline{G}(\mathbf{R}) = E\underline{G}(\mathbf{R}). \tag{9}$$

$\underline{U}(R) \equiv \underline{W}\,\underline{V}(R)\underline{W}^{-1}$ is the diabatic potential matrix whose diagonal elements are the diabatic potential functions, shown in Fig. 2, of the NH^{4+} quasimolecule formed in the collision. The off-diagonal terms of $U(R)$ drive the transitions among the different electronic states. Because $U(R)$ does not depend on the orientation of $\mathbf{R}$, we can simplify Eq. (9) by introducing a partial-wave decomposition for the wave amplitudes $\underline{G}(\mathbf{R})$,

$$G_\gamma(\mathbf{R}) = \sum_{lm} \frac{G_\gamma^{lm}(R)}{R} Y_{lm}(\hat{\mathbf{R}}), \tag{10}$$

where Y_{lm} are spherical harmonics and, in this section, l and m are the quantum numbers for the orbital angular momentum of the relative motion of the nuclei. Inserting Eq. (10) into Eq. (9), we obtain the radial coupled equations

$$\left[\frac{d^2}{dR^2} - \frac{l(l+1)}{R^2}\right] G_\gamma^{lm} - 2\mu\sum_{\gamma'}[U_{\gamma,\gamma'}(R) - E\delta_{\gamma,\gamma'}]G_{\gamma'}^{lm} = 0. \tag{11}$$

The radial functions are independent of the azimuthal quantum number m and satisfy the scattering boundary conditions,

$$\lim_{R\to\infty} G_\gamma^{lm}(R) \to \frac{1}{\sqrt{k_\gamma}}[\delta_{\gamma,\gamma'} j_l(k_\gamma R) + K^l_{\gamma,\gamma'}\eta_l(k_\gamma R)],$$

$$k_\gamma = \sqrt{2\mu[E - U_{\gamma\gamma}(\infty)]} \tag{12}$$

where j_l, η_l are, respectively, the regular and irregular Bessel-Ricatti functions for neutral channels, and the regular and irregular Coulomb functions for the Coulomb channels [17]. $K^l_{\gamma,\gamma'} \equiv K^l$ is a real symmetric matrix, γ' is the index of the incoming channel, and the S matrix is given by

$$\underline{S}^l = (\underline{I} + i\underline{K}^l)^{-1}(\underline{I} - i\underline{K}^l). \tag{13}$$

The cross section for the system to undergo an inelastic transition from state i to j is

$$\sigma(i\to j) = \frac{\pi}{k_i^2}\sum_l (2l+1)|\underline{S}^l|^2_{i,j}. \tag{14}$$

IV. RESULTS AND DISCUSSION

In Fig. 2(a) we display the calculated diabatic potential-energy curves for the triplet states of the NH^{4+} molecular ion. In the figure, the curve for the diabatic state that correlates, in the separated atom limit, to the neutral $N^{4+}+H$ channel crosses the diabatic curves that asymptotically correlate to the energy levels of the N^{3+} ion. Charge transfer occurs when the system, initially approaching in the neutral channel, makes transitions, in regions near the crossings, into the Coulomb channels corresponding to the $N^{3+}(nl;n'l')+H^+$ fragments. These crossings correspond to avoided crossings in the adiabatic picture. Values for the parameters that characterize the major avoided crossings are tabulated in Table IV. In constructing the diabatic energy curves and couplings for $R<13a_0$, we used Eq. (8) and the values for the adiabatic potential curves and couplings given in Tables I and III. At $R=13.71a_0$, the adiabatic potential curves for $(5)^3\Sigma^+$ and $(6)^3\Sigma^+$ states, which correlate to the $N^{3+}(2p3s)$ and $N^{3+}(2p3p)$ states, respectively, share a narrow avoided crossing. Similarly, so do the $(6)^3\Sigma^+$ and the $(7)^3\Sigma^+(N^{4+}(2s)+H)$ adiabatic states at $R>25a_0$ (not shown). The diabatic potentials for $R>13a_0$ were obtained by replacing these, extremely narrow, crossings with real crossings. This procedure was employed in previous calcu-

TABLE IV. Calculated Landau-Zener parameters for selected avoided crossings between adiabatic energy curves for the NH^{4+} ion. States tabulated below cross with the diabatic curve for the neutral $N^{4+}(2s)+H(1s)$ channel, and they are labeled by the atomic quantum numbers of the $N^{3+}(nl;n'l')$ ion to which they correlate. Parameters are defined in the Appendix and expressed in atomic units.

State	Reference	$\Delta E(R^*)$	R^*	$\mathcal{A}(R^*)$	$U_{11}(R^*)$
$^3\Sigma^+(2p3s)$	this calculation	0.000 09	13.71	207	-0.0001
$^3\Sigma^+(2s3d)$	this calculation	0.018	6.99	1.32	-0.007
$^3\Sigma^+(2s3d)$	Ref. [4]	0.02	7.15	≈ 1.1	NA
$^1\Sigma^+(2s3d)$	Ref. [5]	0.012	8.17	2.10	-0.005
$^1\Sigma^+(2s3d)$	Refs. [4,6]	≈ 0.012	8.14	1.27	≈ -0.005

lations [4–6], and we justify it here by appealing to the Landau-Zener-Stueckelberg (LZS) theory [18]. In that theory the probability to make a transition from one adiabatic state to another (at projectile angular momentum l) is (see the Appendix)

$$P_l = \exp(-2\gamma_l),$$

where γ_l is given by Eq. (A6). The parameters, $\Delta E(R^*)$, $\mathcal{A}(R^*)$, corresponding to the avoided crossing at $R^* = 13.71a_0$, are tabulated in the first row of Table IV. Because the crossing is narrow we find, using the values for the LZS parameters given in Table IV, $\gamma_l \approx 0$ and $P_l \approx 1$ for all l, justifying the replacement of the avoided crossing with a diabatic crossing. It follows that the probability $P_l(1-P_l)$ to undergo a charge-transfer transition at $R \approx 13.71a_0$ is negligible.

Equation (9) was integrated using an implementation of the log derivative method of Johnson [19] for collision energies in the range 0.1 eV$<E<$4 keV. Though the quantal close-coupling method is most suited for low collision energies, we extended the calculations into the keV region for the sake of comparison with the results of a semiclassical calculation [4].

The experimental measurements are usually plotted with respect to a mass-scaled energy

$$\frac{E}{\mu} = v^2/2,$$

where v is the relative velocity of the collision system, μ is the reduced mass of the system, and E is the collision energy in the center-of-mass frame. In Figures 3–6, we plot the cross sections with respect to this scaled, center-of-mass energy expressed in units of eV/amu [20].

In Fig. 3(a) we compare the cross sections for capture into the $N^{3+}(2s3d;\ ^1D)$ state given by the previous calculations of Zygelman *et al.* [5] and the calculations of Shimakura, Itoh, and Kimura [4]. Both calculations predict a similar trend in the behavior of the cross sections at higher energies, but the figure reveals a large discrepancy between the two approaches at low collision energies. Whereas the results of Shimakura, Itoh, and Kimura suggest that the singlet cross sections monotonically decrease at energies below 30 eV/amu, the calculation of Zygelman *et al.* gives cross sections that gently rise as the collision energies decrease. The data of Huq, Havener, and Phaneuf also show the definite trend that the total charge-capture cross sections decrease as the collision energy gets smaller. In Ref. [5] it was suggested that the apparent discrepancy between theory [5] and experiment [3] may be the failure in the assumption that, at low energies, the cross sections are independent of the spin multiplicity of the molecular potentials in which the collision partners evolve. However, we did make the strong prediction that the total cross sections for electron capture will eventually rise at sufficiently low collision energies. Below we give a quantitative prediction for the collision energy, below which, the total cross sections again increase.

In Fig. 3(b) we illustrate the cross sections for the same process, capture into the $2s3d$ state of the N^{3+} ion, but in the triplet manifold. The solid line is the result of the present calculation and the dashed line represents the results given in Ref. [4]. Unlike the case for the singlet states, there is relatively good agreement between the two calculations. Both calculations predict a peak in the the cross sections in the vicinity of $\approx 20-30$ eV/amu and they both exhibit prominent undulatory behavior as a function of collision energy. Such oscillations have also been seen in other calculations [5,7,21,22] and are discussed in more detail there. Figures 4(a) and 4(b) compare the results of our calculation and those plotted in Ref. [4], for the capture cross sections in the $N^{3+}(2s3s)$ and $N^{3+}(2s3p)$ levels. For the triplet manifold, we also include cross sections for capture in the excited $N^{3+}(2p3s;\ ^3P^o)$ state. These figures illustrate that the dominant pathway for electron capture, at energies below 10 eV/amu, is the transition into the $N^{3+}(2s3d)$ state. At higher energies transitions into the $N^{3+}(2s3s)$ and $N^{3+}(2s3p)$ levels dominate, the latter becoming the predominant process for energies $E>100$ eV/amu and the former increases steadily as the collision energy increases into the keV region. We notice, in these figures, that there is good qualitative agreement in the cross-section data given in Ref. [4] and the cross sections reported here, though the value in the peak cross section for capture in the $N^{3+}(2s3p;\ ^3P^o)$ state given in Ref. [4] is somewhat greater than that obtained in the present calculation. The qualitative agreement, at high energies, between the two studies is somewhat surprising since they employ distinctly different theoretical methods. The calculations of Shimakura, Itoh, and Kimura use, at energies $E>10$ eV/amu, a semiclassical straight-line trajectory method and include rotational coupling with translation factors, whereas our calculation, valid at low energies, is a fully quantal calculation including only radial coupling without translation factors. Electron translation effects are usually thought to become important at higher collision energies.

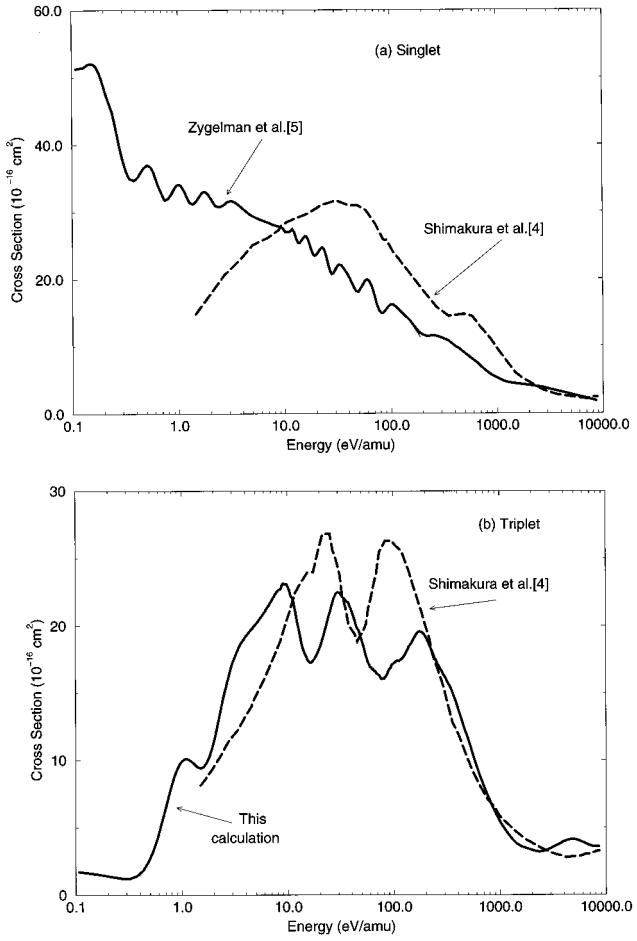

FIG. 3. Cross sections for capture into the $N^{3+}(2s3d)$ states. (a) Singlets. (b) Triplets.

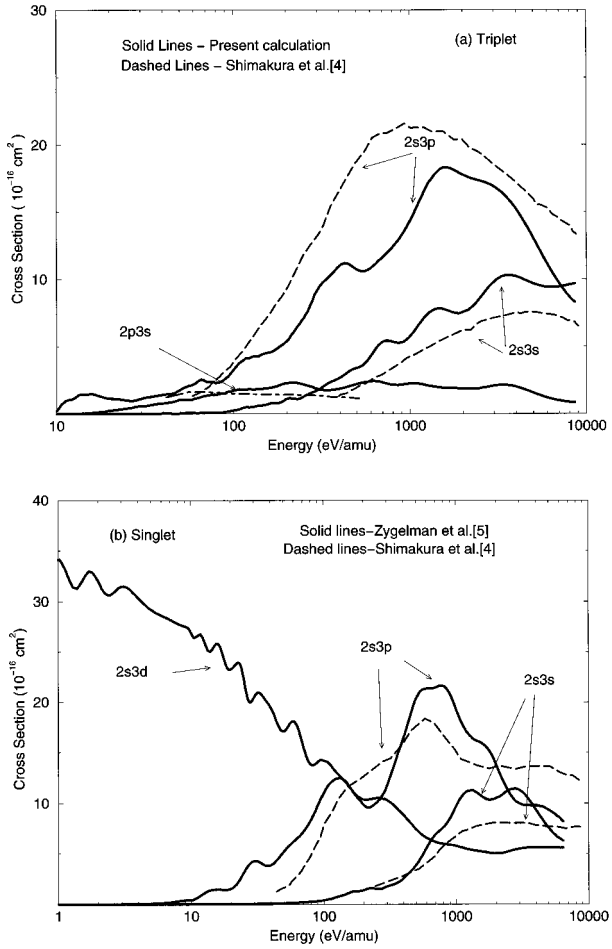

FIG. 4. Calculated cross sections for capture into the $N^{3+}(2l3l')$ states. (a) Triplets. (b) Singlets.

The results of Shimakura, Itoh, and Kimura seem to preclude the possibility for observing Langevin behavior in the NH^{4+} charge transfer system. Folkerts *et al.* [6] pointed out that the results of the calculation of Shimakura, Itoh, and Kimura appears to be in harmony with the experimental data of Huq, Havener, and Phaneuf and suggested that the calculation given in Ref. [5] lacks agreement with the experiment either because the *ab initio* molecular potential method used in that calculation does not command sufficient accuracy, or that the theoretical approach does not include electron translation factors which effectively change the nonadiabatic couplings. Below we show that neither conclusion is warranted.

In Fig. 5, we display and compare the results of our calculation for the total cross sections for capture into the singlet and triplet states of N^{3+} ion, respectively. At energies above $E>30$ eV/amu there are some differences in the cross sections, mainly due to oscillatory structures, but in general they have the same values. However, for collision energies $E<30$ eV/amu the singlet cross sections gently rise whereas the triplet cross sections monotonically decrease as the energy decreases. This behavior is dominated by contributions for capture into the $N^{3+}(2s3d)$ state. In Fig. 3 we presented the cross sections for each spin multiplicity (i.e., the incoming beam is either in a pure singlet or triplet state, respectively) however, the total cross section σ is a statistical sum of the singlet σ_s and triplet σ_t cross sections,

$$\sigma=\tfrac{1}{4}\sigma_s+\tfrac{3}{4}\sigma_t, \tag{15}$$

and the calculated values for σ are given by the solid line in Fig. 5. In Fig. 6 we compare σ with the observed values given in Huq, Havener, and Phaneuf [3] and Folkerts *et al.* [6]. Because of the dominance of the triplet contribution in the sum (15) the total cross sections are effectively quenched in the collision energy region 1 eV/amu$<E<$20 eV/amu.

Figure 6 illustrates the results of our calculation and shows good agreement, at low energies, with the experimental values reported in Refs. [3,6]. The apparent harmony between the measured total cross sections [3,6] and the results obtained here and in Refs. [4,6] is clearly fortuitous. An experimental measurement of the state-to-state capture cross sections [8] might be in a better position to discriminate and test the validity of theoretical predictions.

In Fig. 6 we also illustrate the cross sections obtained when the hydrogen target is replaced with its isotope deuterium. Though the discussions in Refs. [3,4,6] do not distinguish capture rates for the two isotopes (they are used interchangeably in the measurements) we see a small, but discernible, difference for the two cross sections at low energies. At intermediate energies, 30 eV/amu$<E<$1 keV/amu the observations of Refs. [3,6] indicate a prominent peak in the total cross section that is not reproduced in our

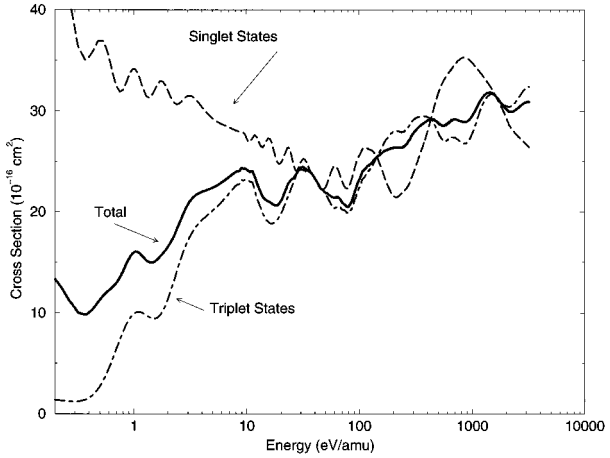

FIG. 5. Partial cross sections for electron capture into triplet states (this calculation) and into singlet states (Ref. [5]). The solid line represents the total capture cross sections and is given by Eq. (15).

calculations. The theoretical calculations of Shimakura, Itoh, and Kimura are in better agreement, but they get a mismatch between the peak observed in the experiments and the peak given by their calculations. However, the error bars displayed in Refs. [3,6], typically $\pm 2.5\times 10^{-16}$ cm^2, correspond to the relative uncertainty, while the total uncertainty is $\pm 5\times 10^{-16}$ cm^2 near the peak. Further, it has been established that a small Rydberg population in the target beam can significantly enhance the total capture yield [13]. While the Rydberg population in the measurements of Ref. [6] was removed down to a principal quantum number $n=12$, the theory of Macek and Ovchinnikov [23] suggests that the remaining Rydberg population could contribute $\sim 2\times 10^{-16}$ cm^2 near the cross-section peak.

To explore the sensitivity of the cross sections on the calculated molecular parameters we resort to the semiclassical LZS theory of charge transfer. In rows 4 and 5 of Table IV we tabulate the LZS parameters reported in Ref. [5] and

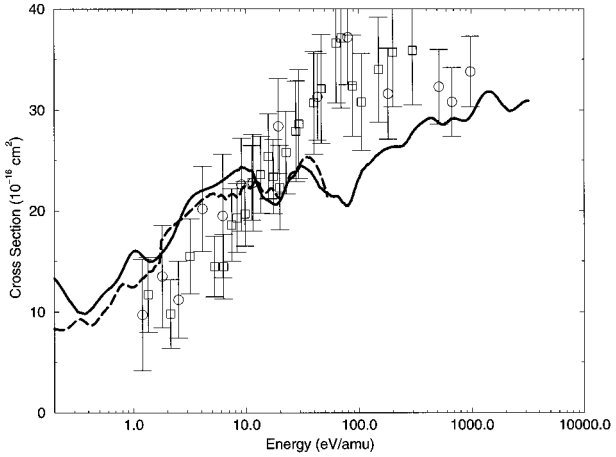

FIG. 6. Comparison of total capture cross sections, corresponding to process (2), and the measured values reported in Refs. [3] (circles) and [6] (squares). Solid line represents hydrogen targets and the dashed line represents deuterium targets.

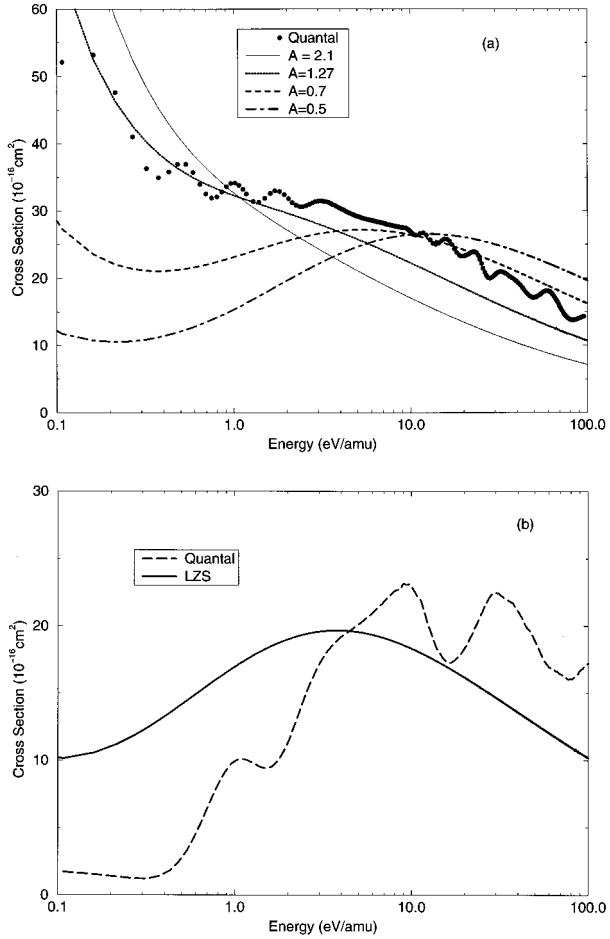

FIG. 7. Partial cross sections, calculated in the LZS approximation, for charge transfer into the $N^{3+}(2s3d)$ states for various values of the nonadiabatic coupling at the avoided crossing distance. Filled circles represent the quantum-mechanical data given in Ref. [5]. (a) Singlet $N^{3+}(2s3d)$ state. (b) Triplet $N^{3+}(2s3d)$ state.

Ref. [4] for the avoided crossing of the $^1\Sigma(2s3d)$ state with the neutral channel. Using Eq. (A1) we calculated the cross sections for charge transfer into the singlet $N^{3+}(2s3d)$ state. The results are plotted with the solid line shown in Fig. 7(a) and they compare favorably with the results obtained by the fully quantum-mechanical coupled-channel approach (solid points) used in Ref. [5]. In this figure, we also plot (dotted line) the results of a LZS calculation using the molecular data given by Shimakura, Itoh, and Kimura [4,6]. The data in Table IV show that the only, significant, difference in the molecular parameters used in the two calculations is the value of the nonadiabatic coupling parameter $A\equiv\mathcal{A}(R^*)$ at the avoided crossing. The cited studies, Refs. [4,6] include translation factors in their formalism and, as a result, the value of the nonadiabatic coupling parameter is effectively reduced to a value of 1.27 a.u. [6], in contrast to the value 2.1 a.u. used in our calculation [5]. Nevertheless, the difference in $\mathcal{A}(R^*)$ translates into a modest effect on the LZS cross sections, as is seen in Fig. 7(a). For successively smaller values for $\mathcal{A}(R^*)$ the resulting LZS cross sections do begin to exhibit the behavior seen in Refs. [4,6] (a positive slope for the cross section as a function of collision energy 1 eV/amu$<E<$30 eV/amu). For the value $\mathcal{A}(R^*)=0.5$, a

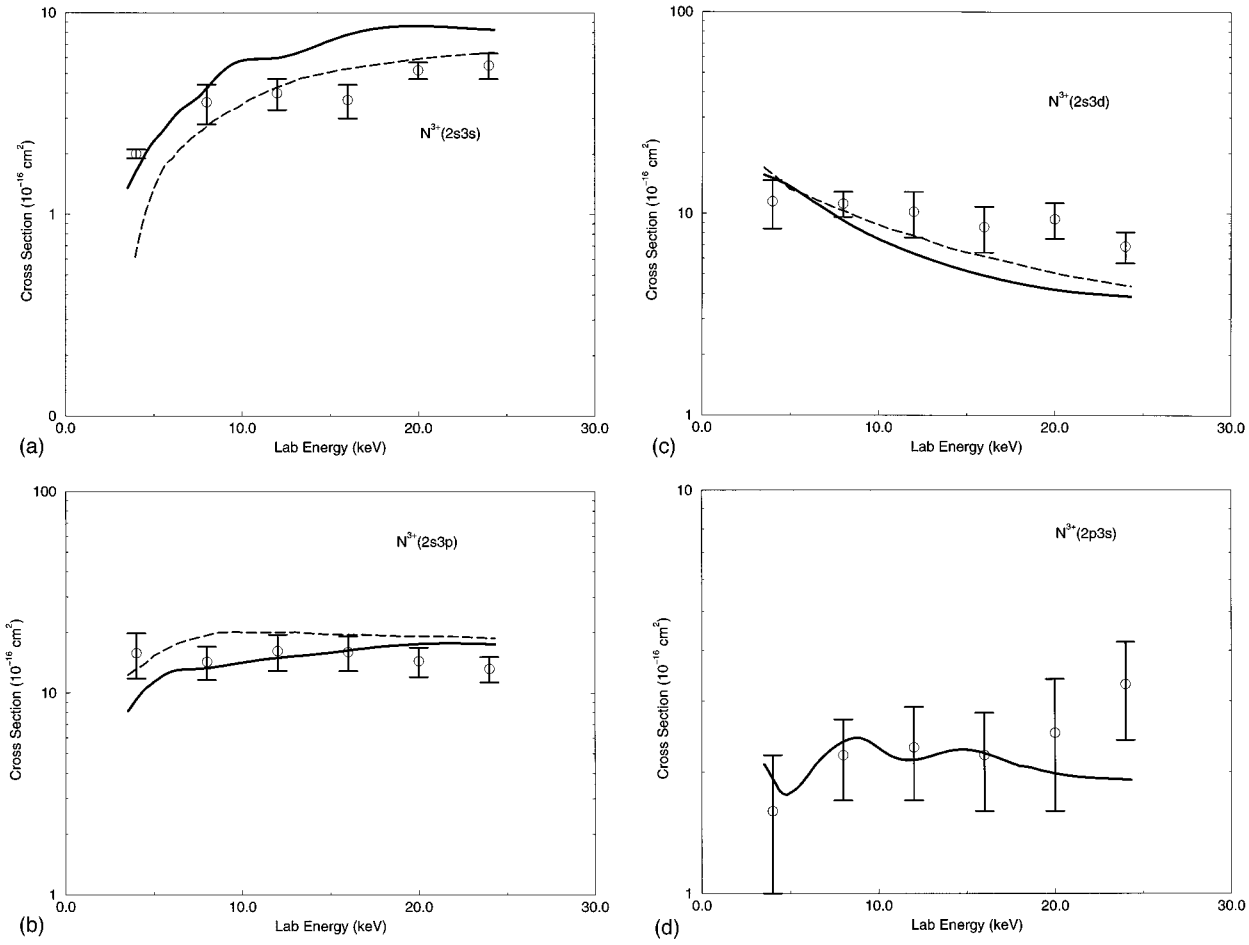

FIG. 8. State dependent cross sections. Solid lines represent the results of this calculation, dashed lines represent data taken from Figs. 3 and 5 in Ref. [4], circles with error bars denote measured data given in Ref. [8]. Capture into (a) $N^{3+}(2s3s)$ state, (b) $N^{3+}(2s3p)$ state, (c) $N^{3+}(2s3d)$ state, and (d) $N^{3+}(2p3s)$ state.

factor of 2 smaller than that reported in Refs. [4,6], we achieve the desired effect.

We contrast the behavior of the singlet cross section with those of the corresponding triplet states. In Fig. 7(b) we repeat the LZS calculation, and compare the results with our quantum-mechanical calculation (dotted line), for capture into the triplet $N^{3+}(2s3d)$ states. Again our LZS results are consistent with the quantal calculation, and they both predict cross sections with positive slopes in the energy region 0.4 eV/amu$<E<$7 eV/amu. They are also in qualitative agreement with the results in Refs. [4,6] [see Fig. 3(b)].

In Fig. 8 we compare our calculated final-state cross sections and the results of the first measurements [8], using energy translation spectroscopy of state-to-state cross sections in this system. In that experiment, nitrogen ions with energy 4 keV$<E(N^{+4})<$24 keV were injected into an oven containing hydrogen. The center-of-mass energy is therefore given by the relation, $E_{\rm cm}/\mu = E(N^{+4})/M$, where $\mu \approx 0.933$ amu is the reduced mass of the NH^{+4} system and $M \approx 14$ amu is the mass of the projectile. In the center-of-mass frame the collision energy spans 250 eV$<E_{\rm cm}<$1.6 keV; outside the range of validity for the PSS approximation. In addition, rotational coupling effects become significant at these energies. However, in Figs. 8(a)–8(d) the calculated cross sections, given by the solid line, are in general good agreement with the experiment for all final-state states considered and for lab energies below 8 keV, with the possible exception of the $N^{+3}(2s3p)$ channel. At 4 keV the measured cross section has the value [8] $(15.8\pm4.0)\times10^{-16}$ cm^2, whereas our calculated value is 9.4×10^{-16} cm^2. At energies greater than 8 keV, the calculated $N^{3+}(2s3p)$, $N^{3+}(2p3s)$ cross sections are in harmony with experiment.

In Figs. 8(a)–8(d) we also transcribe cross sections plotted in Fig. 3 and Fig. 5 of Ref. [4]. These cross sections, calculated using a semiclassical theory, show good agreement with experiments at higher energies.

In conclusion, we have presented theoretical cross sections for electron capture into $N^{3+}(2l,3l')$ due to a low-energy collision of $N^{4+}(2s)$ with $H(1s)$ with a close-coupled quantal method. The results are in qualitative, if not exact, agreement with the previous semiclassical calculations of Shimakura, Itoh, and Kimura [4] for capture into all states except $N^{3+}(2s3d;\ ^1D)$. We find capture into $N^{3+}(2s3d;\ ^1D)$ to manifest Langevin behavior for energies below $\approx$ 10 eV/amu in contradiction to the conclusions of Refs. [4,6]. A parameter study within the Landau-Zener-Stueckelberg approximation, using the molecular data from both groups, confirms Langevin behavior. The total electron-capture cross sections are in good agreement with the merged-beams measurements for energies between 1 eV/amu

and 10 eV/amu, but predict Langevin behavior for energies <0.4 eV/amu. The discrepancy between the previous calculation [5] and experiment [3,6], has been shown to be a breakdown of the assumption that low-energy cross sections are independent of the interaction potential spin multiplicity.

ACKNOWLEDGMENTS

We acknowledge useful discussions with Dr. A. Dalgarno, Dr. C. Havener, and Dr. M. Kimura. This work has been supported by NSF Grant No. OSR-9353227 in Chemical Physics to the state of Nevada. We thank the W. M. Keck Foundation for their generous support and funding of the W. M. Keck Laboratory for Computational Physics at UNLV. Partial support from NASA EPSCoR is acknowledged.

APPENDIX: LANDAU-ZENER-STUECKELBERG APPROXIMATION

In the semiclassical approximation [24] the cross section for charge transfer from state 1(incoming neutral channel) to 2 (outgoing Coulomb channel) is

$$\sigma=\frac{4\pi}{k^2}\sum_l (2l+1)P_l(1-P_l)\sin^2\theta_l \tag{A1}$$

where

$$P_l=\exp(-2\gamma_l),$$

$$\gamma_l=\frac{1}{2}\left[\frac{U_{12}^2}{|dU_{11}/dR-dU_{22}/dR|v_l}\right]_{R=R^*} \tag{A2}$$

and R^* is the radial separation at which the diabatic curves cross. U_{ii} is the diabatic energy for channel i, U_{ij} is the diabatic coupling between channel i and j, $\sin^2\theta_l$ is a phase which we approximate by its mean value 1/2, and v_l is the relative radial velocity of the ion-atom system at internuclear separation R^* given by

$$\mu^2 v_l{}^2=k^2-2\mu U_{11}(R^*)-\frac{(l+1/2)^2}{R^{*2}}. \tag{A3}$$

For a two-channel system the diabatic potentials may be expressed as [25]

$$\begin{aligned}U_{11}(R)&=\epsilon_1(R)\cos^2(\Omega)+\epsilon_2(R)\sin^2(\Omega),\\ U_{22}(R)&=\epsilon_1(R)\sin^2(\Omega)+\epsilon_2(R)\cos^2(\Omega),\\ U_{12}(R)&=U_{21}(R)=[\epsilon_2(R)-\epsilon_1(R)]\sin(\Omega)\cos(\Omega),\end{aligned} \tag{A4}$$

$$\Omega\equiv\int_R^\infty \mathcal{A}(R)dR, \tag{A5}$$

where $\epsilon_i(R)$ is the adiabatic energy for channel i, and $\mathcal{A}(R)$ is the radial nonadiabatic coupling between states i and j. Using this relationship and taking the radial derivatives of the diabatic potentials gives

$$\gamma_l=\frac{\pi}{16}\left|\frac{\Delta E(R^*)}{\mathcal{A}(R^*)}\right|\frac{1}{v_l}. \tag{A6}$$

For a two-channel system the LZS cross section is determined by three parameters that characterize the molecular potentials, $\Delta E(R^*)$ the energy defect of the adiabatic potential curves at R^*, $\mathcal{A}(R^*)$ the value of the nonadiabatic coupling at R^*, and v_l the radial velocity of the relative motion at R^* with angular momentum $\hbar l$. This velocity is also sensitive to the value of the diabatic energy $U_{11}(R^*)$. We make the additional approximation of replacing the internuclear separation for an avoided crossing with the value R^*.

[1] S. E. Butler and A. Dalgarno, Astrophys. J. **241**, 838 (1980).
[2] C. A. Feickert, R. J. Blint, G. T. Surrat, and W. D. Watson, Astrophys. J. **286**, 371 (1984).
[3] M. S. Huq, C. C. Havener, and R. A. Phaneuf, Phys. Rev. A **40**, 1811 (1989).
[4] N. Shimakura, M. Itoh, and M. Kimura, Phys. Rev. A **45**, 267 (1992).
[5] B. Zygelman, D. L. Cooper, M. J. Ford, A. Dalgarno, J. Gerratt, and M. Raimondi, Phys. Rev. A **46**, 3846 (1992).
[6] L. Folkerts, M. A. Haque, C. C. Havener, N. Shimakura, and M. Kimura, Phys. Rev. A **51**, 3685 (1995).
[7] P. C. Stancil and B. Zygelman, Phys. Rev. Lett. **75**, 1495 (1995).
[8] R. W. McCullough, T. K. McLaughlin, J. M. Hodgkinson, and H. B. Gilbody, Nucl. Instrum. Methods Phys. Res. B **98**, 199 (1995).
[9] F. P. Keenan, C. A. Ramsbottom, K. L. Bell, A. Berrington, A. Hibbert, W. A. Feibelman, and W. P. Blair, Astrophys. J. **438**, 500 (1995).
[10] A. D. Silber, S. F. Anderson, B. Margon, and R. A. Downes, Astrophys. J. **462**, 428 (1996).
[11] In Fig. 4 of Ref. [3], the theoretical data of Feickert *et al.* [2] are displayed and compared to the measured cross-section data. It appears to show good agreement between theory and experiment. However a careful comparison of the theoretical data plotted in Fig. 4 of Ref. [3] and the data given in Figs. 6(a) and 6(b) and 7(a) and 7(b) in Feickert *et al.*, suggests that the two sets of displayed theoretical data are consistent only if the former authors used the conversion $E(\text{eV/amu})\approx E_{\text{cm}}(\text{eV})/14$ amu, where $E(\text{eV/amu})$ is the collision energy given by the abscissa in Fig. 4 of Ref. [3], and E_{cm} is the center-of-mass energy (used in the calculation of Feickert *et al.*). Instead, the experimental data are plotted with respect to the collision energy $E_{\text{cm}}(\text{eV})/\mu$, where $\mu\approx 0.93$ amu is the reduced mass of the $N^{4+}H$ ion-atom system, and not 14 amu, the mass of the nitrogen atom [12]. Taking this correction into account the comparison between theory [2] and experiment is fair.
[12] R. Phaneuf (private communication).
[13] C. C. Havener, F. W. Meyer, and R. A. Phaneuf, in *Proceedings of the Seventeenth International Conference on the Physics of Electronic and Atomic Collisons* (Institute of Physics

and Physical Society, Bristol, 1991), p. 381.
[14] C. E. Moore, *Atomic Energy Levels*, Natl. Bur. Stand. Ref. Data Ser., Natl. Bur. Stand. (U.S.) Circ. No. 35 (U.S. GPO, Washington, D.C., 1971).
[15] This equation corrects a typographical error in Eq. (27) of Ref. [5].
[16] We ignore additional terms proportional to the inverse of the nuclear reduced mass.
[17] *Handbook of Mathematical Functions*, edited by M. Abramovitz and A. Stegun (Dover, New York, 1965).
[18] This analysis makes the central assumption that the effects of the long-range avoided crossings can be accounted for by the semiclassical LZS theory. A more refined, quantum-mechanical treatment should be carried out in order to test the validity of this assumption at low collision energies.
[19] B. R. Johnson, J. Comput. Phys. **13**, 445 (1973).
[20] In Fig. 6 of Ref. [5] we plotted the calculated singlet charge-transfer cross sections and compared them to the measured values for the total, charge capture cross sections reported in Ref. [3]. In transcribing the measured cross sections, in this figure, we erroneously assumed that the cross sections given in Ref. [3] are tabulated with respect to the values E/M, where M is the mass of the nitrogen nucleus (see [11]).
[21] P. C. Stancil, B. Zygelman, N. J. Clarke, and D. L. Cooper, Phys. Rev. A **55**, 1064 (1997).
[22] P. C. Stancil, B. Zygelman, N. J. Clarke, and D. L. Cooper, J. Phys. B **30**, 1013 (1997).
[23] J. Macek and S. Y. Ovchinnikov, Phys. Rev. Lett. **69**, 2357 (1992).
[24] M. F. Mott and H. S. W. Massey, *The Theory of Atomic Collisions* (Clarendon, Oxford, 1965), Chapt. XIII.
[25] F. T. Smith, Phys. Rev. **179**, 111 (1969); T. G. Heil, S. Butler, and A. Dalgarno, Phys. Rev. A **23**, 1100 (1981).